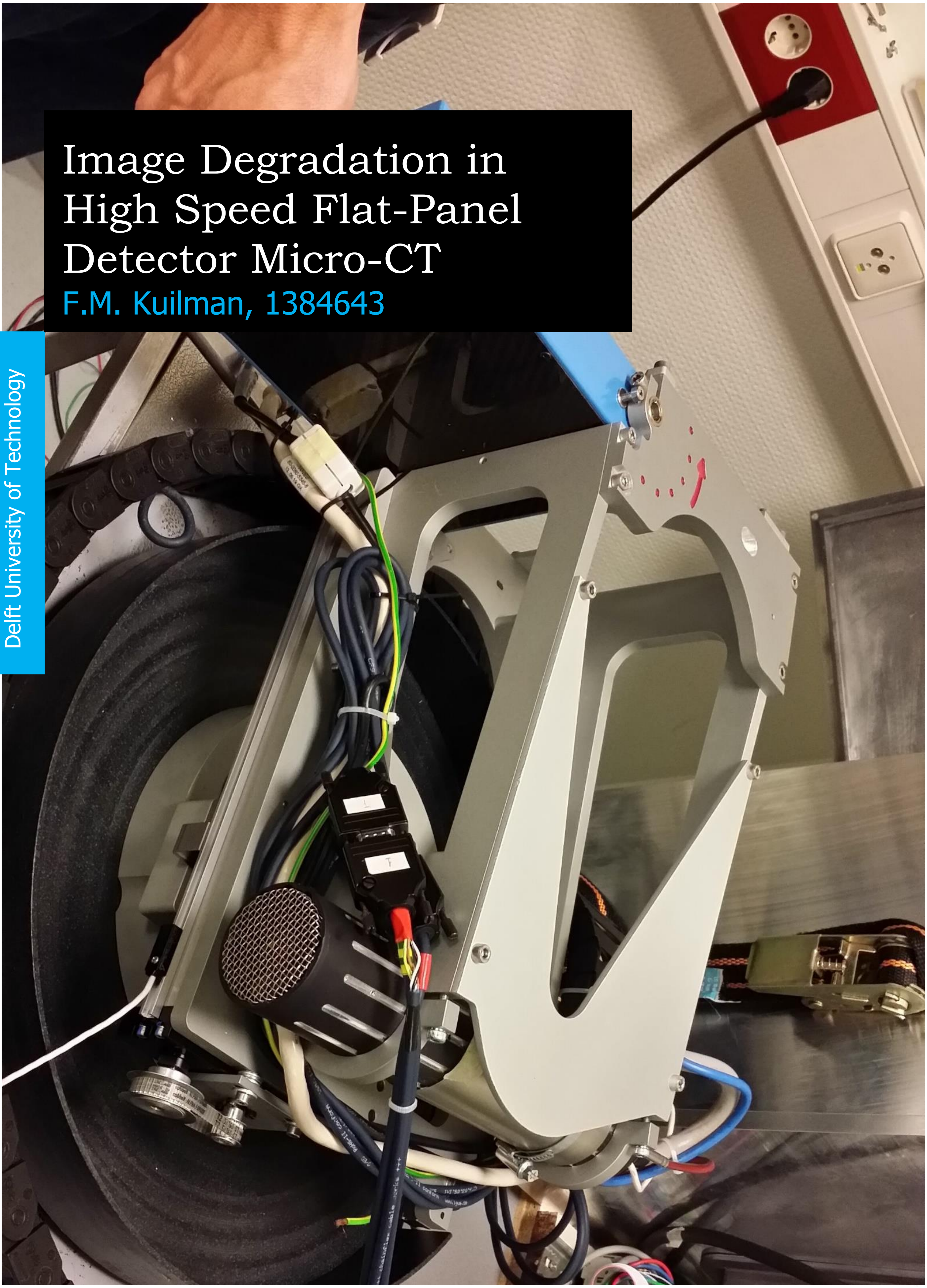

Image Degradation in High Speed Flat-Panel Detector Micro-CT

F.M. Kuilman, 1384643

Delft University of Technology

TU Delft Delft University of Technology

Challenge the future

Image Distortion in Fast Flat-Panel Detector micro-CT

By

F.M. Kuilman

In partial fulfilment of the requirements for the degree of:

Master of Science
in Biomedical Engineering

at the Delft University of Technology,
to be defended publicly on Tuesday June 30, 2015 at 10:00 AM.

Supervisors:	Prof. Dr. F. J. Beekman	
	Dr. C. Wu	
Thesis committee:	Prof. Dr. F. J. Beekman,	TU Delft
	Dr. ir. M.C. Goorden,	TU Delft
	Dr. J. Kalkman,	TU Delft

An electronic version of this thesis is available at http://repository.tudelft.nl/.

Abstract

Flat-panel detector micro-CT is a promising new tool for small animal imaging, and becomes important for in vivo studies of small animals for developing new drugs and therapies.

The aim of this report is to investigate the best possible image quality for high-speed flat-panel detector micro-CT. Specifically, the aim is to investigate the severity of image distortion as a result from the high rotational and acquisition speed. The best possible acquisition mode for high-speed micro-CT is investigated by scanning a (deceased) mouse and investigating the required scan time and resulting image quality. Image degradation due to afterglow and due to the rolling shutter effect are determined by measuring the signal intensity decay profile of the detector and by measuring the angle deformation of a pipe phantom for various speeds.

A total scan time of 15 seconds was possible for a 2x2-binning Continuous Rotation scan while acquiring 144 projections, where the 1x1-binning Step & Shoot scan took 6:55 min while acquiring 1440. This lead to a decrease in image quality resulting from the higher pixel-binning and the lower number of acquired projections. At the fastest image acquisitions speeds used in this report, afterglow might cause slight image degradation. After 103 ms, which is also the time intervals between acquiring projections during the 15 s scan (quickest scan done on the deceased mouse) 7% of the original intensity was measured in the detector. This could be partly caused by the shutdown behavior of the X-ray source, and no influence of afterglow was found in the other measurements. Hence, it is unlikely that afterglow causes serious image degradation at the speeds used in this report. However, further research with dedicated devices should be done to better estimate the effect of Afterglow at these high acquisition speeds. The Rolling Shutter Effect at a rotation speed of 24 and 40 degrees per second did not cause an angular deformation large enough to require correction, as the maximal deformation was only 0.00288 degrees per mm.

Based on these results, there are no image corrections needed for any motion-induced image degradation discussed in this study at the rotation speeds used in this report.

Contents

1

Introduction

Computed Tomography (CT) is a very hot topic of research, with CT speed and quality improving rapidly over the years. With an estimated 62 million CT scans in 2007 in the United States alone, CT has become one of the main diagnostic tools for clinical use worldwide [1]. An example of a more recent innovation is the Dual-Source CT: a CT scanner with two distinct X-ray sources instead of one, allowing for faster and higher quality imaging [2].

Besides clinical CT systems, there are also CT systems that employ micro-focal-spot X-ray sources and high resolution detectors for preclinical applications. They allow for very high resolution imaging with pixel sizes within the micrometer range; CT Imaging within this range is called Micro-CT. Micro-CT has proven to be very important in small animal imaging because the anatomical structures of small animals are very tiny when compared to humans: very high resolution images are needed to properly image these anatomical details. Micro-CT offers a minimally invasive way to perform longitudinal studies throughout the lifetime of a small animal, which are essential in the development of new drugs and therapy for humans [3] [4] [5].

The **aim** of this research is to use flat-panel detectors in very fast micro-CT scans and to correct for artefacts resulting from these high speeds if necessary. The set-up used in this report is the CT subsystem from the VECTor^{4}CT (Fig. 1.1) [6] and U-SPECT^{4}CT scanners being built by MILabs (Utrecht, The Netherlands). These scanners are built to image small animals using several different image modalities (SPECT/PET/CT).

Figure 1.1: The VECTor^{4}CT. Image courtesy of MILabs.

1.1. Fast micro-CT

There are various reasons why a very short scan time is important in small animal micro-CT. First of all: the faster the CT scan can be done, the shorter the subject is exposed to (harmful) radiation. Hence, if the same voltage and current are used in the X-ray source (with no changes to the delivered dose per time), shorter scan times result in a lower radiation dose to the subject. This is important in small animal research as even low radiation doses can affect immune response and other biological pathways [7]. This can alter experimental outcomes in longitudinal studies. Secondly, the temporal resolution of a CT scanner is determined by the gantry speed and volume coverage of the detector [8]. Increasing the speed of the gantry causes a higher temporal resolution, which allows for a higher sampling rate when tracking contrast agents through a subject.

1.2. Cone-Beam Computed Tomography

In cone-beam computed tomography (CBCT) the X-rays emit out of the X-ray source in a cone shape to irradiate the surface of the detector, this is the case in the flat-panel set-up used in this report. An illustration of the CBCT set-up with the axes of the system can be seen in Fig. 1.2a. The system consists out of an X-ray source and a flat-panel detector, both of which are attached to a gantry which allows for rotation. Note that in most real CT systems the axis of gantry rotation (Z-axis) is horizontal, allowing patient or animal to lie down on a bed inside a system.

The subject is placed between the X-ray source and detector. The intensity of X-rays radiating the detector depends on the amount of attenuation by the subject. The higher the attenuation, the lower the intensity of X-rays reaching the detector which leads to a lower read-out value on the detector. When the detector is read out, it results in a 2D image or projection. This is in contrast to the conventional fan-beam CT detector arrays which capture only a single row (1D) at a time (Fig. 1.2b). The 2D acquisition of CBCT allows for full volume coverage in a single rotation of the gantry [9] while for fan-beam CT multiple rotations at different positions along the Z-axis are needed to cover the entire volume.

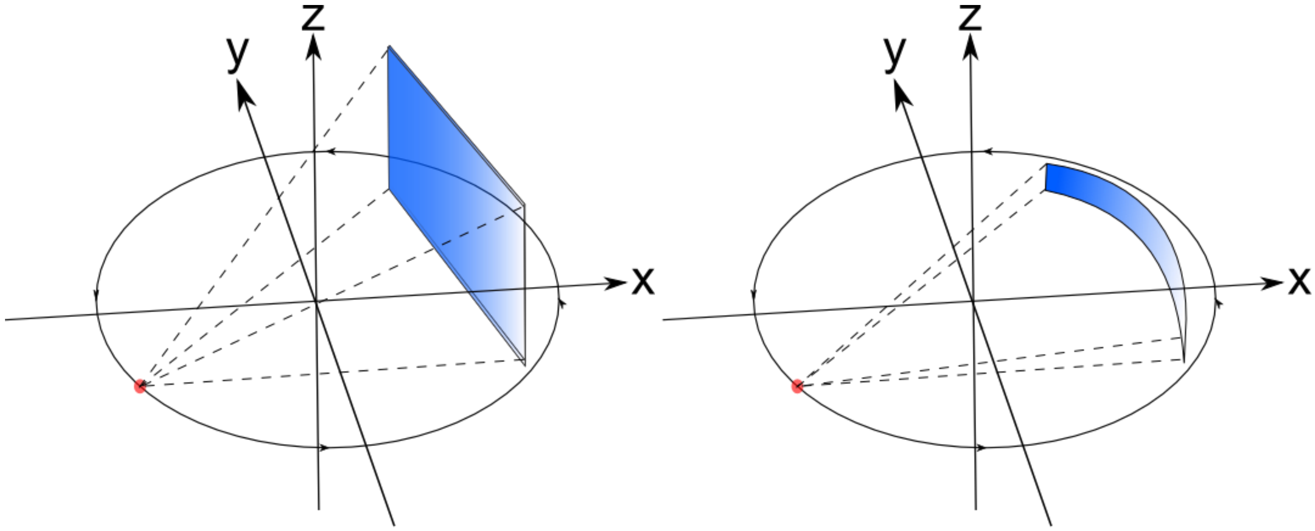

(a) (b)

Figure 1.2: The set-up of a CT system. (a) Shows a CBCT set-up such as the one used in this report, this set-up acquires multiple rows of pixels per acquisition (2D). (b) Shows a conventional fan-beam CT set-up, this set-up only acquires a single row of pixels per acquisition (1D). The red dot is the X-ray source and the blue square on the right is the flat-panel detector. The axes of the system (X,Y,Z) are given.

1.3. Flat-Panel Detectors

A flat-panel detector is the part of the CT set-up that does the measurements: it converts the energy it receives from the X-ray photons into an electric signal which can be read-out. It consists out of several parts. The scintillator is the part which absorbs the X-ray photons and emits the received energy in the form of optical (lower energy) photons [9]. These photons are then absorbed by the Complementary Metal Oxide Semiconductor (CMOS) which converts them into a charge which can be read out. The CMOS integrates the signal over a time period (the integration time) which is reset at the start of each measurement period during normal measurements [10].

Flat-panel detectors can have high resolutions, allowing for the possibility of use in micro-CT. When compared to conventional fan-beam 1D detector arrays, flat-panel detectors are able to cover a much larger volume per rotation but have a slower acquisition time [3] [9].

1.4. Volume Reconstruction

The image captured on the detector for a certain gantry angle is called a projection. The projections acquired are simple gray-scale images, i.e. a matrix containing discrete values. The value stored for an element in the detector (corresponding to a pixel in the image) correspond to the amount of radiation that was received by the element during the integration time. As both the pixel intensity I_p measured by the detector when an object is placed and the pixel intensity I_0 measured by the detector if no object is present are known, the amount of attenuation can be determined using the Beer-Lambert law [12]. The Beer-Lambert law gives relationship between the intensity and absorption:

$$I = I_0 e^{-\int \mu \, dl} \qquad (1)$$

Here *dl* is the distance the X-ray travels through the subject with an attenuation of μ. Inserting the known values into Eq. 1 and taking the logarithm gives:

$$\ln\left(\frac{I_p}{I_0}\right) = -\sum_n^i \mu_i d_i \qquad (2)$$

Here $\ln\left(\frac{I_p}{I_0}\right)$ is called the raysum as it contains the amount of absorption per ray.

From all the projections acquired during a CT scan a volume can be reconstructed. A reconstructed volume is a 3D matrix consisting of a number of volume elements (called voxels) of a fixed pre-determined size, each having a value which corresponds to the attenuation of that particular voxel. The raysum can be seen as the total absorption of all the voxels a ray passes between source and detector [12]. For each projection, the raysum is spread out (backprojected) over all the voxels the ray passes between the X-ray source and detector. Note that there are several different methods to spread the raysum over the voxels [12].

Backprojection will lead to a blurred reconstruction, as each point from the object will be spread out over the reconstructed volume. To correct for this, a ramp filter (Fig. 1.3) is applied to all the projections. The ramp filter reduces blur (low frequencies) while maintaining sharp features (high frequencies). This process is known as ‘filtered backprojection’. Note that backprojecting a single projection does not result in a useful reconstructed volume, but results in the projection being spread out over the volume [12]. The original volume is only properly reconstructed when many different projections (at many different projection angles) are backprojected.

To reconstruct a volume from all the acquired projections, different reconstruction algorithms can be used. In fan-beam CT, which uses a 1D detector row, the X-rays spread out in a fan shape when travelling from source to detector. This fan-shape causes each consecutive pair of rays from the source to the detector to have a difference in angular interval. However with such geometry it is easy to see that the fan beam projections can be rearranged into parallel beam projections. Therefore the filtered backprojection can be used when taken this into account [13].

For CBCT a frequently used reconstruction algorithm is the Feldkamp-Davis-Kress (FDK) algorithm (and its variations), which is based on filtered backprojection method [11]. FDK is the reconstruction method used in this report and is an extension of the algorithm for the 1D fan-beam reconstruction into 2D cone-beam reconstruction. In FDK a pre-weighted filter is applied to the backprojection. This pre-weighted filter is used to correct for the distance on the detector from the central ray in the cone. After applying the pre-weighting and ramp filter, all projections are backprojected along their respective trajectory. This reconstructs a volume of which the size is defined by the number of voxels and the chosen voxel size.

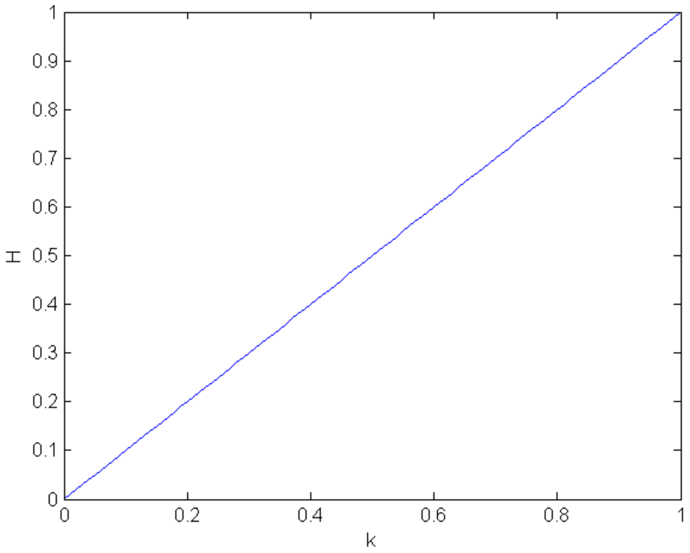

Figure 1.3: A ramp filter in the frequency domain.

If the number of projections used in reconstruction is n and the number of voxels reconstructed is m^3, the computational complexity scales with nm^3 [14]. The number of voxels used is typically very large, hence the computational cost or time needed to do reconstruction is typically large. However, FDK can be done in parallel to a large degree [14], this makes running FDK on GPU's feasible, which can significantly reduce the time required for reconstruction [14].

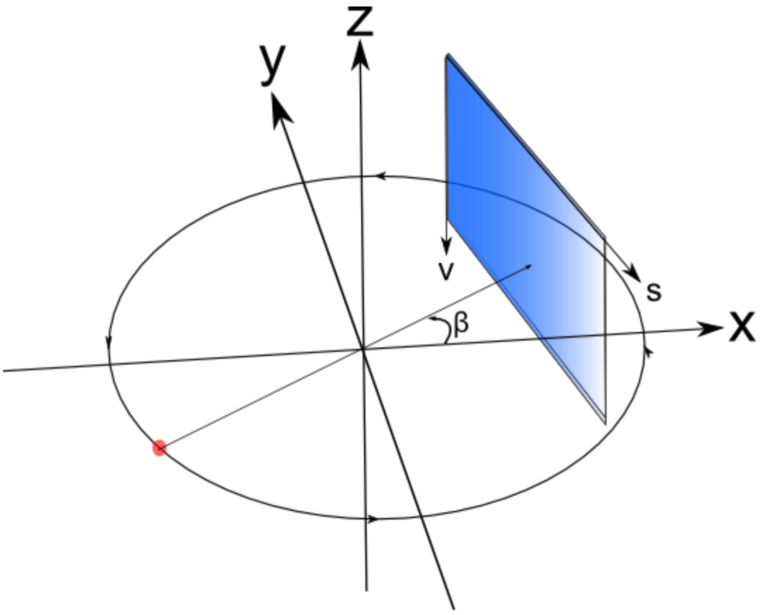

Figure 1.4: The set-up of the system with parameters. The red dot is the X-ray source and the blue square on the right is the flat-panel detector. The axes of the system (X,Y,Z) are given, as is the angle of the projection β and the position along the Flat-Panel Detector (s, v)

1.5. Acquisition mode

There are two possible methods of acquiring projections: Step & Shoot and Continuous Rotation.

Step & Shoot is an intuitive method of image acquisition. Firstly, the X-ray source is turned on and the detector is then cleared of charge. A projection is made. The CT gantry (the rotating part containing both the detector and the X-ray source) is then rotated with a fixed increment. Again the charge is cleared and another projection is made. This process is repeated until projections are acquired over an angular range of at least 180 degrees plus the cone angle; the minimum required for reconstruction [15]. However, there is a disadvantage of using Step & Shoot as the CT gantry needs to stop and start for each projection acquired. This results in a long scan time and hence a higher total delivered dose to the subject being exposed to radiation during the entire scan time.

A Continuous Rotation scan starts by turning on the X-ray source. The gantry is brought up to the desired speed and the detector is cleared of charge. As the detector is rotating a projection is made. After a fixed increment, the detector charge is cleared and another projection is made; this is repeated until projections are acquired over at least 180 degrees plus the cone angle [15]. This method is faster than the Step & Shoot method, resulting in a lower dose. The disadvantage of using this method is that acquisition is performed during rotation of the CT gantry, which means that the projections may be degraded by motion artefacts. Depending on the amount of motion artefacts, correction may be needed [16].

A comparison between these two methods of rotation was done by Kerl et al. [16]. Kerl used a flat-panel detector with 1888 by 1408 pixels and used 2x2 binning. With this set-up a decrease in scan time from 50 minutes for Step & Shoot to 40 seconds for Continuous Rotation was achieved. This speed-up factor of 75 was possible without significantly reducing image quality. This speed-up resulted in a decrease in radiation dose from 4.127 Gy to 0.067 Gy, a factor of 61.6 .

However, the usage of Step & Shoot by Kerl differs from the usage of Step & Shoot in this report, as Kerl turns off the X-ray source after each projection and turns it on again before the next. Due to the lower time the subject is exposed to radiation, this could possibly lead to a smaller total radiation dose. However, each projection will require additional time for the X-ray source to be turned on again which could add to the total radiation dose and will cause Step & Shoot to be a more time consuming method when implemented this way.

1.6. Motion-Induced Image Degradation

Image degradation in CBCT can be caused by a variety of causes. The main concern in this report is the image degradation arising as a consequence of the characteristics of the flat-panel detector together with the high-speed rotation of the CT gantry. This can lead to the image degradation as a result of afterglow and the rolling shutter effect.

The CsI(Tl) Scintillator used in the flat-panel detector has a slower decay behavior than a conventional CT detector array. Very fast acquisition may lead to ‘afterglow’: this is caused by the previous image still being slightly visible in the new image. The manufacturer stated that it might take up to several minutes before all charge has decayed. In the reconstructed volume this could lead to shading and ring-like artefacts.

Rolling Shutter is a method of image capture where an image is not captured simultaneously throughout the image, but on a row by row basis instead as shown in Fig. 1.5 This means that the pixels acquired in the read out direction of the capture device do not correspond to the exact same point in time; as each row is read out in consecutive order, each row will correspond to a later point in time.

This means that when capturing fast motion, row by row read out of pixels at high rotational speeds will distort the projections acquired, as the entire projection does not correspond to a single time in the motion. A demonstration of the Rolling Shutter Effect can be seen in Fig. 1.6 Here the Rolling Shutter Effect causes a straight line in the object space parallel to the Z-axis to appear angled on the detector because the object is moving relative to the detector while the projection is acquired.

In the case of a CT gantry rotating fast during acquisition, the projections are distorted by the relative motion of the gantry to the object being scanned. In this case, the CT gantry will have rotated slightly further for each row being read out. This means that each consecutive row that is being read out will represent a slightly different position in space, or as the CT gantry is rotating, correspond to a different angle. This means that a straight line in the object space parallel to the Z-axis will appear angled on the projection (as exampled in Fig. 1.6). When performing a full CT scan each acquired projection will have this deformation. When doing the volume reconstruction this will lead to a volume twisted along the Z-axis.

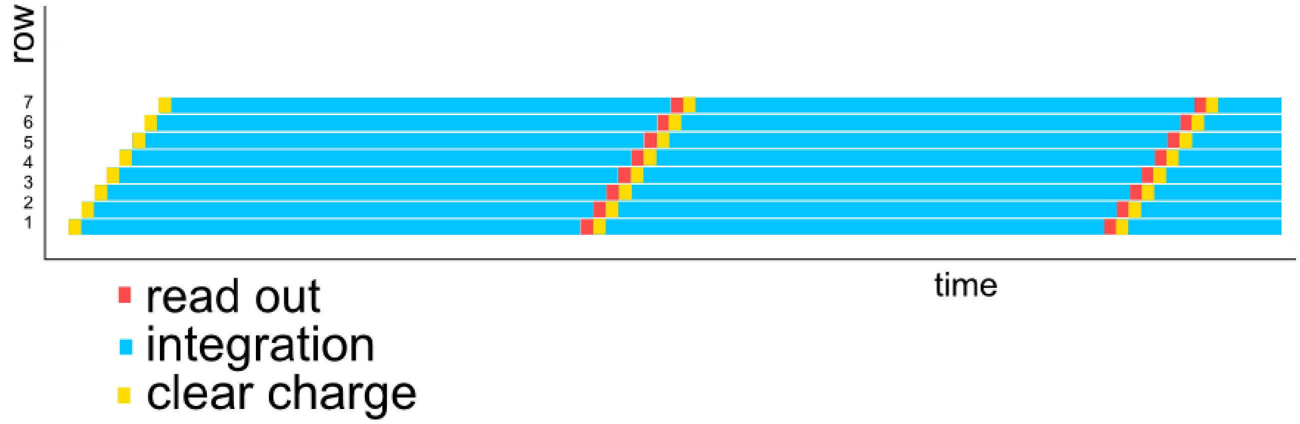

Figure 1.5: An illustration of non-simultaneous read-out of rows. The red parts illustrate the moments in time when a row was being read out, the blue parts illustrate the time over which integration takes place and the yellow parts illustrate where the charge is cleared in the detector for acquiring the next image. This causes each row to contain data from a slightly different moment in time.

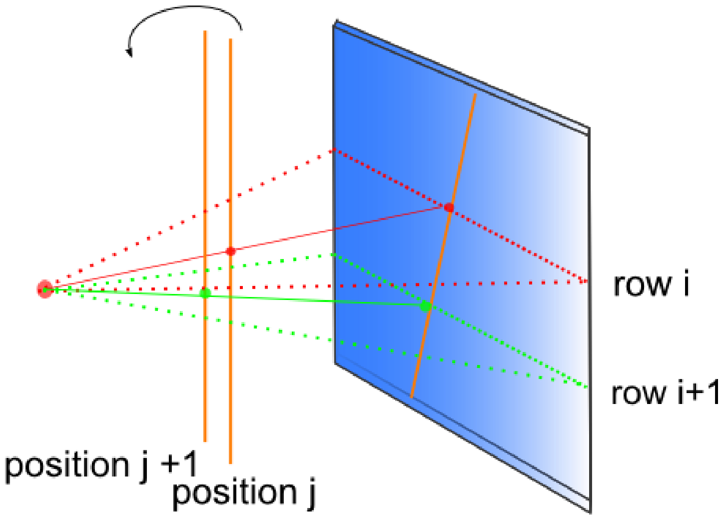

Figure 1.6: A demonstration of the Rolling Shutter Effect. This is best demonstrated by taking the reference frame which rotates along with the CT gantry, this means that in the selected reference frame the object appears to be rotating. The rolling shutter effect causes a straight line in the object space parallel to the Z-axis (the orange line, shown at two distinct positions) to appear angled on the detector as the object is moving while the projection is acquired.

1.6. Outline of the Report

The **aim** of this research is to investigate the feasibility of high speed flat-panel detector micro CT and to what extent these high speeds cause image degradation and whether a correction is necessary. This report is organized into chapters as follows:

Chapter 1 gives an introduction on the subject of CT scans, flat-panel detectors and image reconstruction.
Chapter 2 goes into detail on the used set-up.
Chapter 3 discusses the method used to gather data.
Chapter 4 gives the results of the measurements.
Chapter 5 discusses the results and suggests what future research should be performed.
Chapter 6 summarizes the most important conclusions of this report.

2

Materials

The set-up used consists out of a flat-panel detector and an X-ray tube which are both attached to the CT gantry which is able to rotate around an object to be imaged. The acquired projections are reconstructed into a volume using a computer running reconstruction software. The entire set-up used is shown in Fig. 2.1.

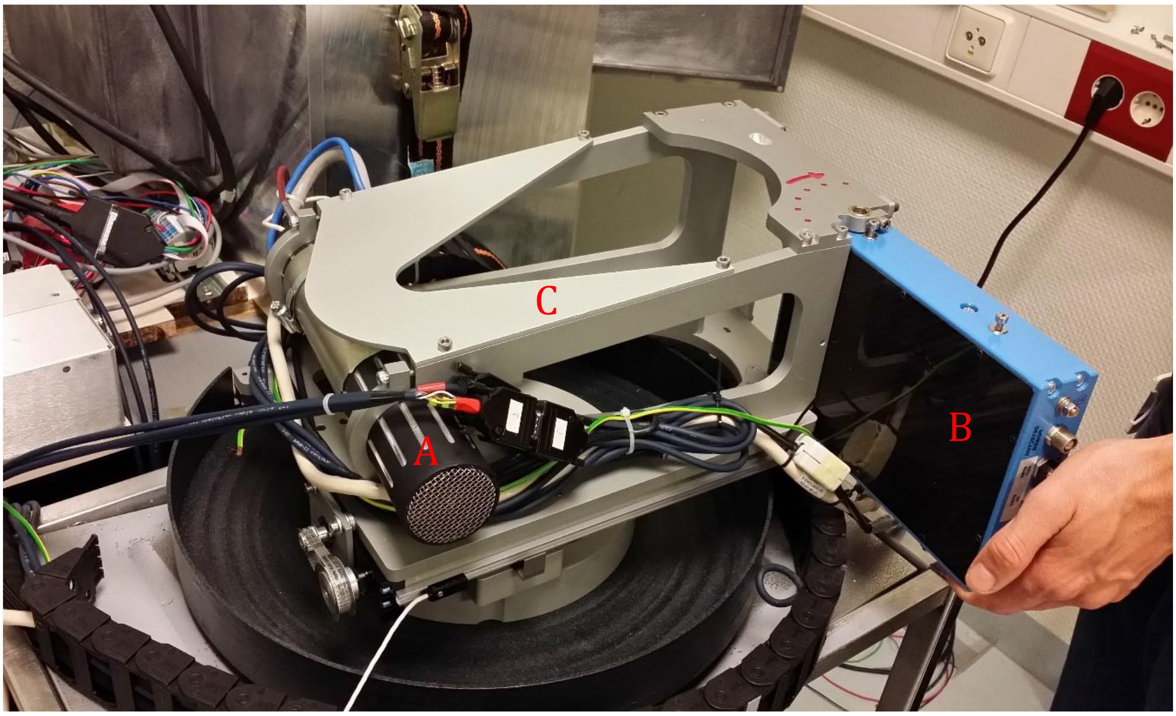

Figure 2.1: The used set-up without housing. The X-ray tube is marked 'A' and the flat-panel detector is marked 'B' which are both attached to the gantry which is marked 'C'. For scanning an object, it should be placed between the X-ray tube and detector.

2.1. Flat-Panel Detector

The flat-panel detector used is a PerkinElmer Dexela 1512 and is shown in Fig. 2.2. This is a CMOS flat-panel detector able to measure at a maximum frame rate of 26 frames per second (Dexela Limited, PerkingElmer, UK) [17]. It uses an CsI(Tl) scintillator and has a switchable pixel gain so it can be used for CT imaging as well as for static imaging with high dynamic range. The detector has a maximum resolution of 1944 x 1536 pixels, the maximum frame rate for this setting is 26 fps, which means an image can be acquired every 38 ms. It has a sensitive area of 145.4 x 114.9 mm and a pixel pitch (distance between the center of the first pixel to the center of the next pixel) of 74.8 µm [17].

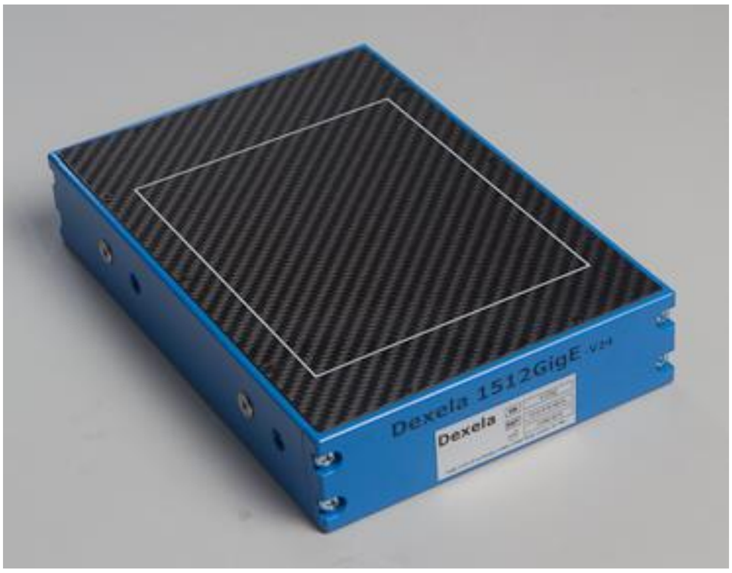

Figure 2.2: The Dexela 1512 flat-panel detector. Image: courtesy of PerkinElmer.

2.2. X-ray tube

During the making of this report, the CT scanner has been under construction. This resulted in two different x-ray tubes used in the measurements done. The specifications of both X-ray tubes are given in Table 2.1 (RTK, Germany). Turning the X-ray tube on and off is not an instantaneous process. The X-ray tube needs to be warmed up before it can be properly used to image the object. It also takes a short while (up to ~0.5 s) for the X-ray source to stop emitting radiation after being switched off.

Table 2.1: The specifications of the used X-ray tubes.

Tube model	RTW MCBM 65M-70x50 W 40	RTW MCBM 65M-30x20 W 40
Emission angle	44°	49.8°
Peak energy	10 – 65kVp	10 – 65kVp
Max power	30W	12W
Max current at 50kV	1mA	0.24mA
Max current at max voltage	0.7mA	0.18mA
Spot size	70×50µm	30×20µm
Filters	Al 0.5mm	Al 0.5mm

2.3. The Gantry

The gantry contains the X-ray source and flat-panel detector. The distance of the X-ray source to the detector is fixed, but the distance of the X-ray source to the center of rotation can be altered (this will also alter the distance between the center of rotation and flat-panel detector). This allows for a variable magnification factor. The specifications of the gantry used in all the measurements is given in Table 2.2.

Table 2.2: The specifications of the used set-up

Distance X-ray source to center of rotation	163.72 mm
Distance X-ray source to the detector	273.34 mm
Maximum gantry rotational speed	80 degrees/second

2.4. Reconstruction Software

In this report the FDK implementation from Reconstruction Toolkit (RTK) [18] was used. RTK is an open-source cross-platform software package for fast circular CBCT reconstruction based on the Insight Toolkit (ITK) [19] and written in C++. It can run on GPUs using the CUDA architecture.

RTK first pre-processes the projections. In this step the logarithm of images is calculated so that the attenuation can be determined as is given by Eq. 2. Then the images are weighted to correct for the displacement of the detector from the center of the X-ray beam and angle of the detector if there is any. Then the FDK algorithm is performed. A Hann-window was added in the ramp filter step.

3

Method

3.1. Rotation Mode Measurements

The Rotation Mode measurements are done to find the differences between Step & Shoot and Continuous Rotation, of interest are the quality of the acquire reconstructions and the time required to perform the scan using these different modes. To find the differences, scans over a full rotation are done on a (deceased) mouse using different parameters. The settings are shown in Table 3.1. The ‘RTW MCBM 65M-30x20 W 40’ X-ray tube was used, the specification of this tube is given in Table 2.1.

Table 3.1: The different measurements done on a mouse at different speeds using step & shoot (S&S) and continuous rotation (CR).

#	Mode	Frame averaging	# projections	binning	Speed (degree /s)	Step (deg)	Integration time (ms)
1	S&S	1	1440	1x1		0.25	80
2	S&S	1	360	1x1		1	80
3	S&S	1	288	1x1		1.25	80
4	S&S	1	144	1x1		2.5	80
5	S&S	1	144	2x2		2.5	40
6	CR	1	144	2x2	12	2.5	80
7	CR	1	144	2x2	20	2.5	40
8	CR	1	144	2x2	24	2.5	40

The difference in total scan time and the corresponding image quality resulting from these measurements can be used to determine reduction in image quality for faster scan times. The volumes are reconstructed using a 0.05 mm voxel size. To quantify the image quality of the reconstructed volumes, the background-noise and signal-to-noise-ratio of tissue (tissue-SNR) is calculated. This is done by calculating the average pixel value and standard deviation for a part of the background of the reconstructed volume, and by calculating the average pixel value of a uniform part of the reconstructed image where a tissue is present. The tissue-SNR can now be calculated by using Eq. 3.

$$SNR = \frac{mean(signal) - mean(background)}{standard\ deviation(background)} \qquad (3)$$

3.2. Afterglow Measurements

To determine the extent of the image degradation in the projections caused by afterglow, the decay profile of the CsI(Tl) scintillator has to be determined. This is done by acquiring projections without rotating the CT gantry and without an object being present between detector and source. This will result in projections where the intensity is a direct result of the exposure to the X-ray source and to residual charge left in the scintillator (afterglow).

For these measurements, the X-ray source is first warmed up. After it has fully warmed up, several projections are made. The intensity of these projections determine the peak read-out value (i.e. the maximum value the projections will have in a normal operation). Then the source is turned off while continuously acquiring projections.

If present, dead pixels on the detector can be corrected for by attributing the average pixel value of its neighboring pixels to the dead pixel. In the raw images black rows will be present due to the read-out mechanics of the detector, for the purpose of the afterglow measurements these rows can simply be removed. The average pixel value of each projection is calculated by calculating the mean of all the pixels values in the projection. Each average pixel value is plotted to its corresponding time value, which will give the decay profile of the detector.

The background intensity is measured by acquiring several images before the X-ray source is turned on. Averaging the pixel values of these projections, will result in the background intensity.

To have a low as possible time resolution in the acquired decay profile, a short integration time should be used and a higher pixel binning, to allow for faster read out.

All projections and raw images (without any form of pre-correction) for the afterglow measurements are acquired using an integration time of 12 ms. The raw projections are acquired at 4x4 binning (486 x 384), at 14 bit unsigned integers. For these measurements the ‘RTW MCBM 65M-30x20 W 40’ X-ray tube of which the specifications are given in Table 2.1 was used.

3.3. Rolling Shutter Effect Measurements

To determine the amount of image degradation caused by the rolling shutter effect, two different measurements are needed. First of all, a measurement of an object undisturbed by the rolling shutter effect is required. This measurement should be captured using the Step & Shoot mode. The second measurement needed is a measurement of the same object but now disturbed by the rolling shutter effect. It is easiest to measure the image difference if the deformation due to the rolling shutter effect is largest. This is the case for a continuous rotation measurement with the rotation speeds set as high as possible. All measurements are reconstructed into volumes with a voxel size of 0.12 mm.

The phantom used for these measurements is a steel hollow pipe (Fig. 3.1). The pipe is 85.0 mm long, has an outer diameter of 4.0 mm and a wall thickness of 1.0 mm. It has attenuation coefficients large enough to almost completely block out X-rays passing straight through the center of the pipe phantom. This will cause the pipe phantom to appear solid in the reconstruction (although being hollow). The advantage of having a large attenuation is that the object can be segmented out of the reconstructed volume using a threshold on the pixel values. The center of the pipe can then be determined, by calculating the center of mass of the pixels above the threshold.

Figure 3.1: The pipe phantom used in the rolling shutter effect measurements.

The measurements that were done on the pipe phantom are given in Table 3.2. For these measurements the ‘RTW MCBM 65M-70x50 W 40’ X-ray tube of which the specifications are given in Table 2.1 was used.

The reconstruction of the volumes is done such so the center pixel in the reconstructed image is also the center of rotation, allowing for easy calculations. The method used to calculate the volume twist is shown in Fig. 3.2. The colored dots are the positions of the center of mass of the pipe phantom. Position i and j refer to a difference position along the z-axis of the same measurement (or a different slice in the reconstruction) and angles α_i and α_j are the angles these positions make with the horizontal line through the center of rotation. Hence, (α_{iCR} - α_{iGS}) is the angle difference for a position i. This angle difference is calculated for each reconstructed slice. A linear regression is performed of the angle difference (α_{iCR} - α_{iGS}) against the Z-position of slice i using an ordinary least squares estimator. This linear regression is given by:

$$\Delta\alpha = \gamma Z + \beta + \varepsilon_i \qquad (4)$$

Here γ is the slope of the regression. This slope is the relation between the angular deformation (α_{iCR} - α_{iGS}) and the length along the Z-axis and is thus a measure for image degradation due to the rolling shutter effect. β is the intercept (the value where the regression line crosses the $\Delta\alpha$-axis), which is the difference between α_{iCR} and α_{iGS} at slice z=0, due to slightly different starting position of the gantry in scans with different rotation mode. And ε_i is a (random) error variable. Hence the measured amount of angular deformation ($\Delta\alpha$) is given by the regression γ times the length along the Z-axis (Z) plus the intercept β and error ε_i.

For a comparison between different Continuous Rotation measurements, only the slope γ needs to be compared. I.e. any offset arising from a different starting position of the gantry for different measurements is not relevant to the deformation.

Table 3.2: The measurements done on a pipe phantom.

#	Mode	# Projections	Binning	Speed (degree/s)	Step (degree)	Integration time (ms)
1	S&S	960	1x1		0.375	80
2	CR	240	2x2	24	1.5	40
3	CR	148	2x2	40	2.43	40

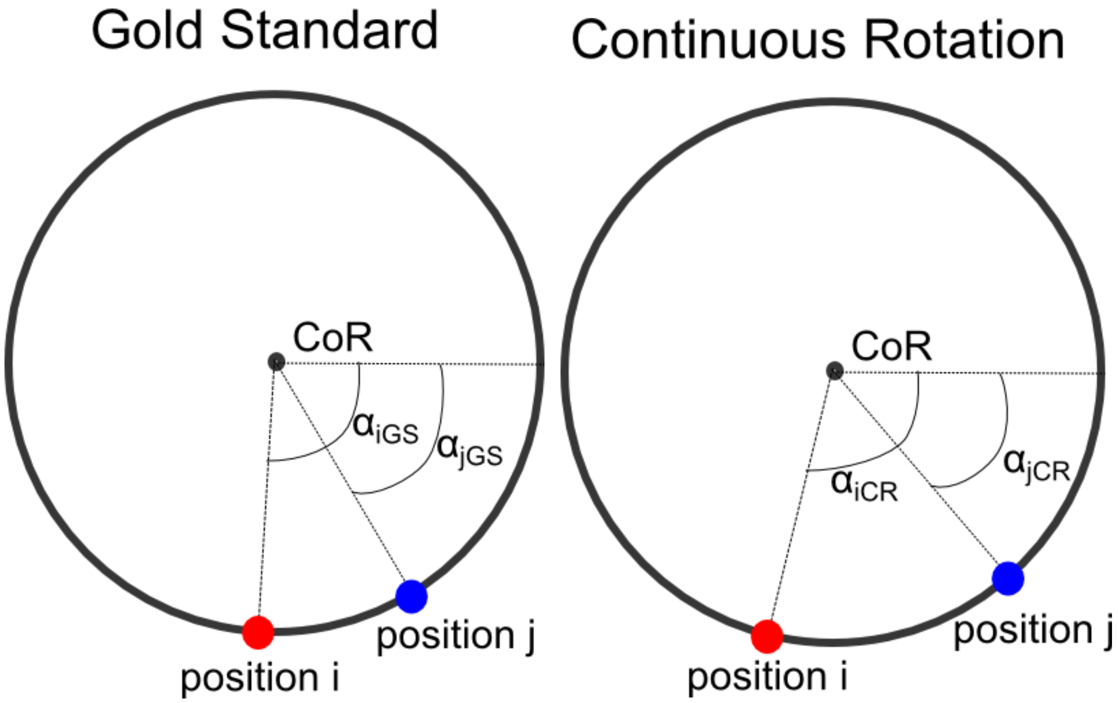

Figure 3.2: The angles used in the angle measurements. The center pixel in the reconstructed image is also the center of rotation. The colored dots are the positions of the center of mass of the pipe phantom. Position i and j refer to a difference position along the z-axis of the same measurement (or a different slice in the reconstruction) and angles α_i and α_j are the angles these positions make with the horizontal line through the center of rotation. Hence, (α_{iCR} - α_{iGS}) is the angle difference for a position i. This angle difference is calculated for each reconstructed slice and a linear regression is performed to determine the relation between the angular deformation (α_{iCR} - α_{iGS}) and the length along the Z-axis (this is the slope of the regression).

4

Results

4.1. Acquisition Mode

The measurements done on the deceased mouse and total scan time are shown in Table 4.1. The highest imaging quality is achieved in measurement 1, which is selected as the gold standard for the sake of this comparison. It had a total scan time of 6:55 min and 1440 projections were acquired during this scan. The fastest scan done was measurement 8, therefore this measurement is selected as the standard measurement for fast scans.

Table 4.2: The different scans done on a mouse and the resulting scan time. Measurement number 1 is chosen as the gold standard, as it is the highest quality image achieved by these measurements.

#	Mode	Frame averaging	# projections	binning	Speed (degree /s)	Step (deg)	Integration time (ms)	Scan time (min)
1	S&S	1	1440	1x1		0.25	80	6:55
2	S&S	1	360	1x1		1	80	2:10
3	S&S	1	288	1x1		1.25	80	1:55
4	S&S	1	144	1x1		2.5	80	1:11
5	S&S	1	144	2x2		2.5	40	1:00
6	CR	1	144	2x2	12	2.5	80	0:30
7	CR	1	144	2x2	20	2.5	40	0:18
8	CR	1	144	2x2	24	2.5	40	0:15

The first acquired projections of both runs are given in Fig. 4.1. Axial slices of the reconstructed volume are given in Fig. 4.2. The tissue-SNR is calculated using Eq. 3 using the areas A, B, C and D given in Fig. 4.2. The resulting tissue-SNR is 10.4 dB for the gold standard and 7.9 dB for the fast run.

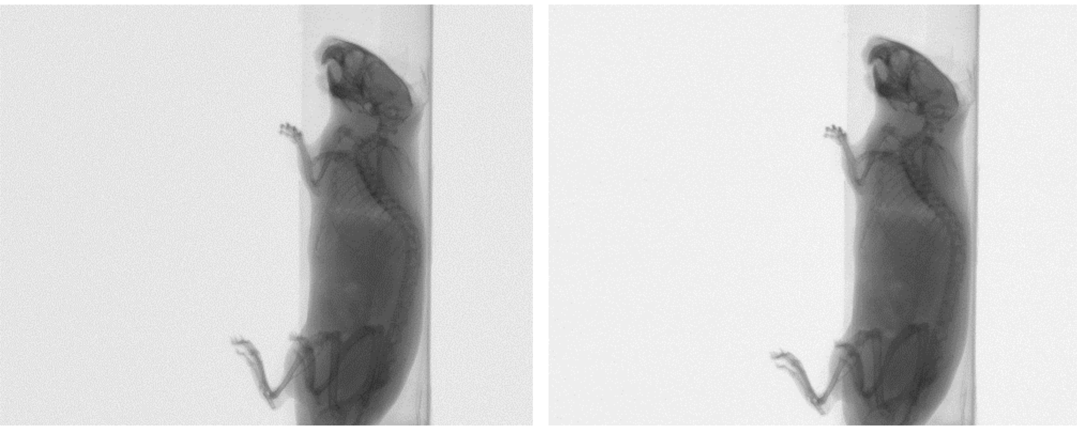

Figure 4.1: Acquired projections used in the reconstructions. On the left is first projection acquired during the Gold Standard run. On the right is the first projection acquired during the Fast run. The difference in integration time has been corrected for.

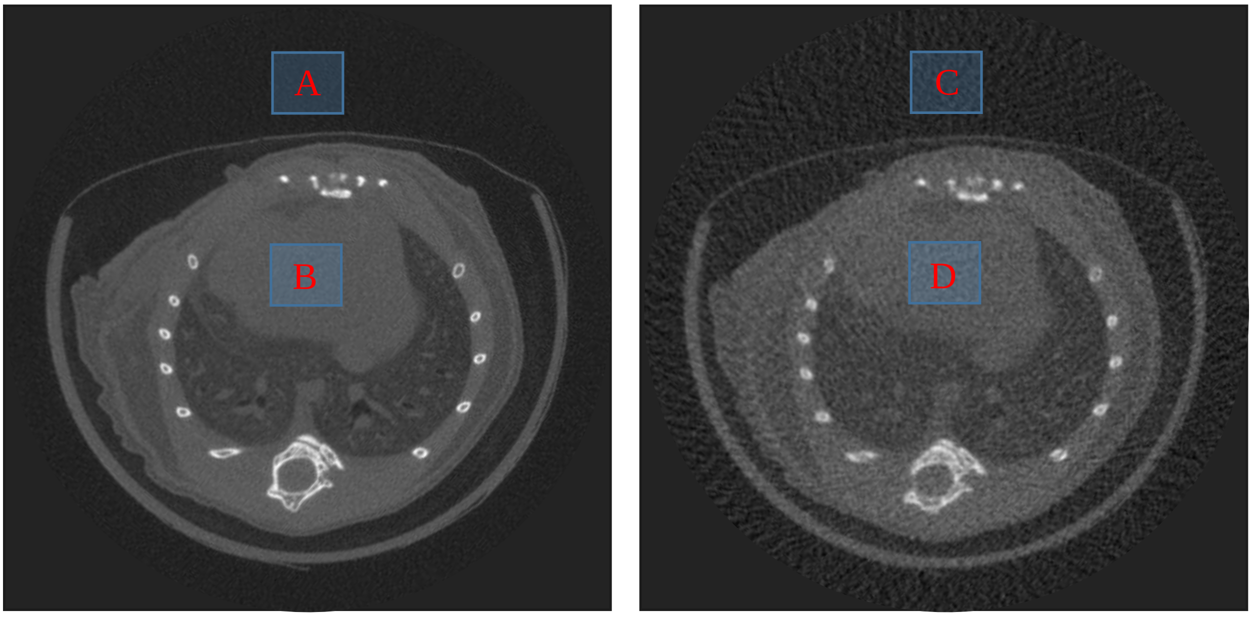

Figure 4.2: Axial slices of the reconstructed volumes. On the left is an axial slice of the Gold Standard Reconstructed volume, on the right is an axial slice of the Fast run (15s, 144 projections at 2x2 binning). The squares indicated by the letters A,B,C and D are the areas used to calculate the tissue-SNR, where A en C are used to calculate the background intensity and standard deviation, B en D are used to calculate the tissue intensity.

4.2. Afterglow Measurements

To be able to measure the afterglow the detector is irradiated by the X-ray source for several seconds without an object present between the source and detector. After this, the X-ray source is turned off. The afterglow is now measured by continuously acquiring projections directly after the X-ray source is turned off.

A raw image acquired while the X-ray source was turned on is seen in Fig. 4.3. An example of a dead pixel is indicated by the red circle. This dead pixel is corrected for by attributing the average value of the neighboring pixels to this dead pixel. The black rows which can be seen in Fig 4.3 are a result of the read out mechanics of the detector and are simply removed from the results.

The intensity is measured by averaging the pixel values for each projection and is given as a percentage of the original intensity (the intensity before turning of the X-ray source). The results of the afterglow measurement are given in Fig. 4.4. Note that Fig. 4.4 has an exponential y-axis and the red line gives the background intensity, measured by acquiring projections before the X-ray source was turned on and calculating the average pixel value for these projections. The intensities of the first several measurements points before the X-ray source was turned off are given in Table 4.2.

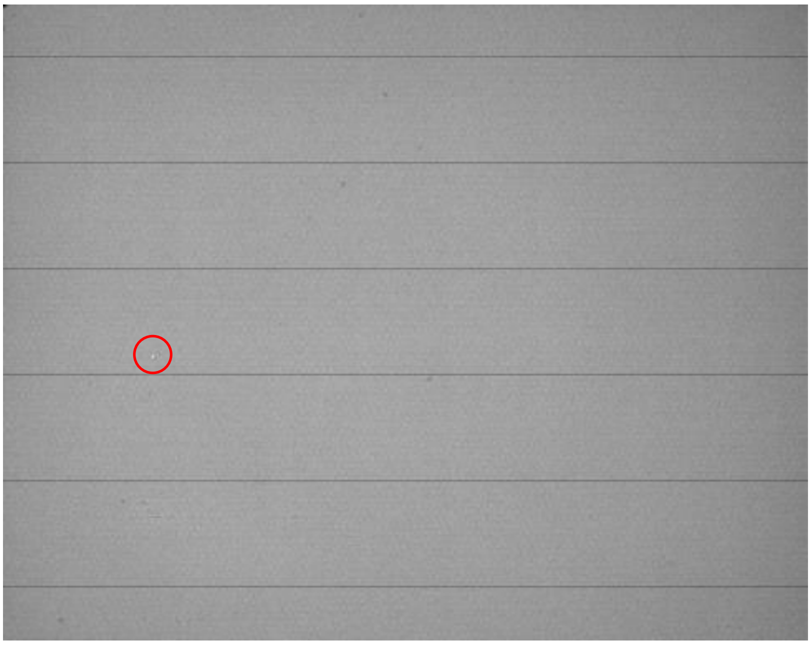

Figure 4.3: The raw detector image without an object present between X-ray source and detector. Note the black lines on the detector (a result of the read out mechanics) and one dead pixel indicated by the red circle.

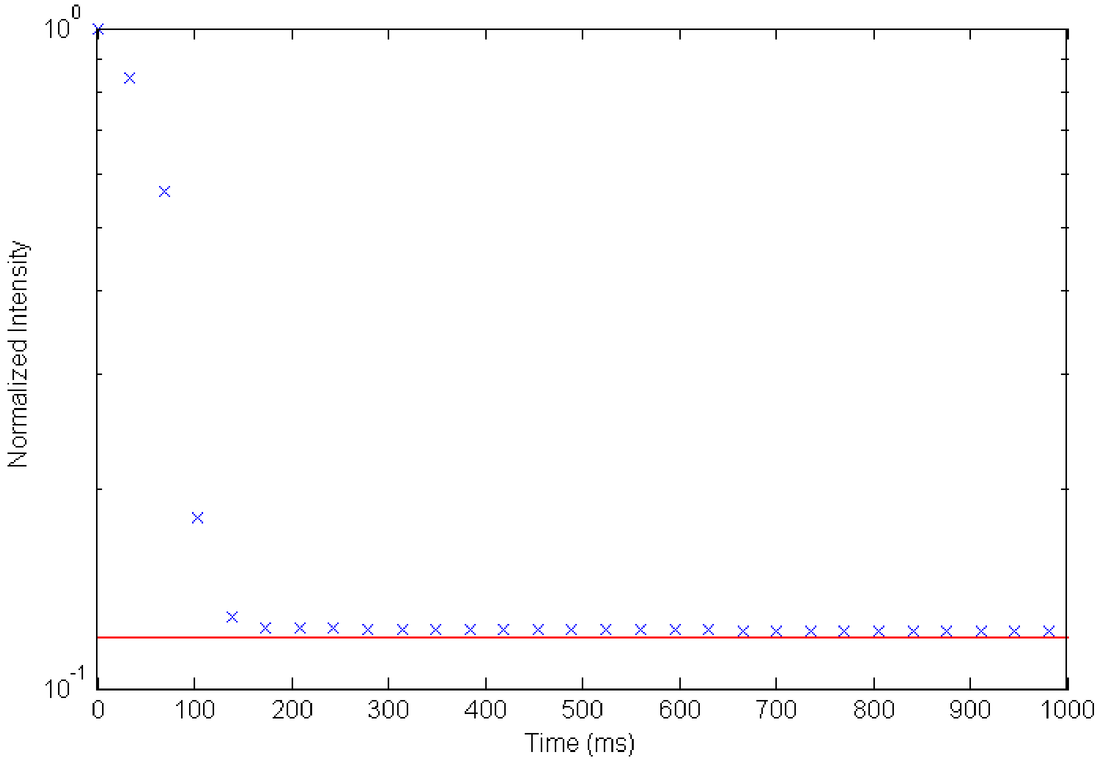

Figure 4.4: The measured decay profile of the PerkinElmer Dexela 1512 after turning the X-ray source off. The red line shows the background radiation. The intensity is given as a factor of the intensity right before the X-ray source was turned off. The data is acquired using a stationary set-up. The source is turned off at t=0 after it had been on for several seconds.

Table 4.2: The first few measurements of the decay profile, the results are given as a percentage of the intensity at t=0 and the background value is subtracted from the results, 0% means the intensity is at the background level.

Time (ms)	Intensity (percentage of intensity at t=0)
0	100
33	81
68	51
103	7.1
138	1.0

4.3. Rolling Shutter Effect Measurements

The resulting scan times for the measurements done on the pipe phantom are given in Table 4.3. An axial slice of the pipe phantom image is given in Fig. 4.5, the red ‘x’ in this pictures indicates the center of mass of the pipe phantom found by using the method described in section 3.3.

The angles measured on every transaxial slice over the entire volume using the method shown in Fig. 3.2, they are given in Fig. 4.6. The angles of the reconstructed volumes of the continuous rotation scans minus the angle of the Gold Standard and the corresponding linear fits are given in Fig. 4.7. The results of the linear fits are given in Table 4.4. The slope of the linear fits of all the continuous rotation measurements is shown in Fig. 4.8.

Table 4.3: The measurements done on the pipe phantom with the resulting total scan times.

#	Mode	Number of Projections	Pixel Binning	Speed (degree/s)	Step (degree)	Integration time (ms)	Scan time
1	S&S	960	1x1		0.375	80	4:14
2	CR	240	2x2	24	1.5	40	0:15
3	CR	148	2x2	40	2.43	40	0:09

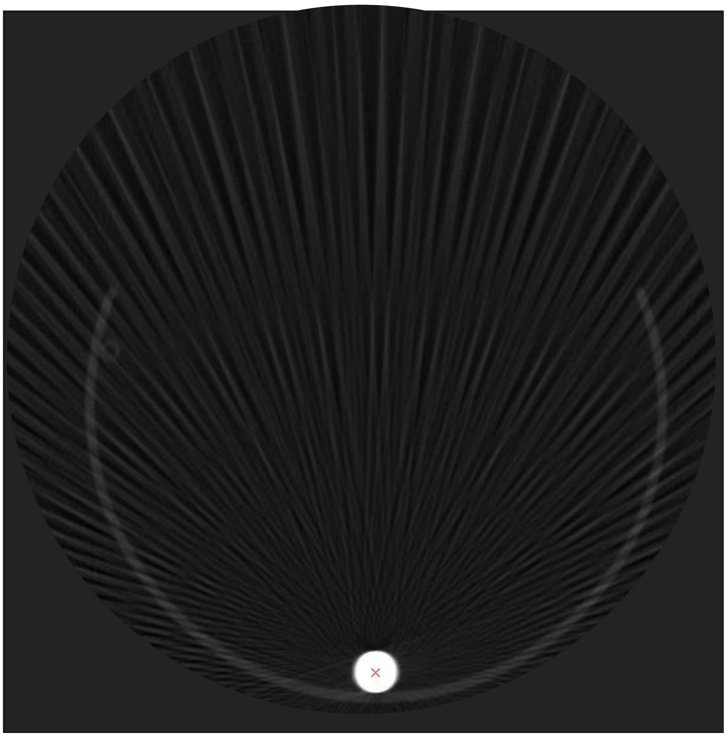

Figure 4.5: An axial slice of the reconstructed phantom volume. The red x indicates the center of mass of the pipe phantom found by the method described in section 3.3.

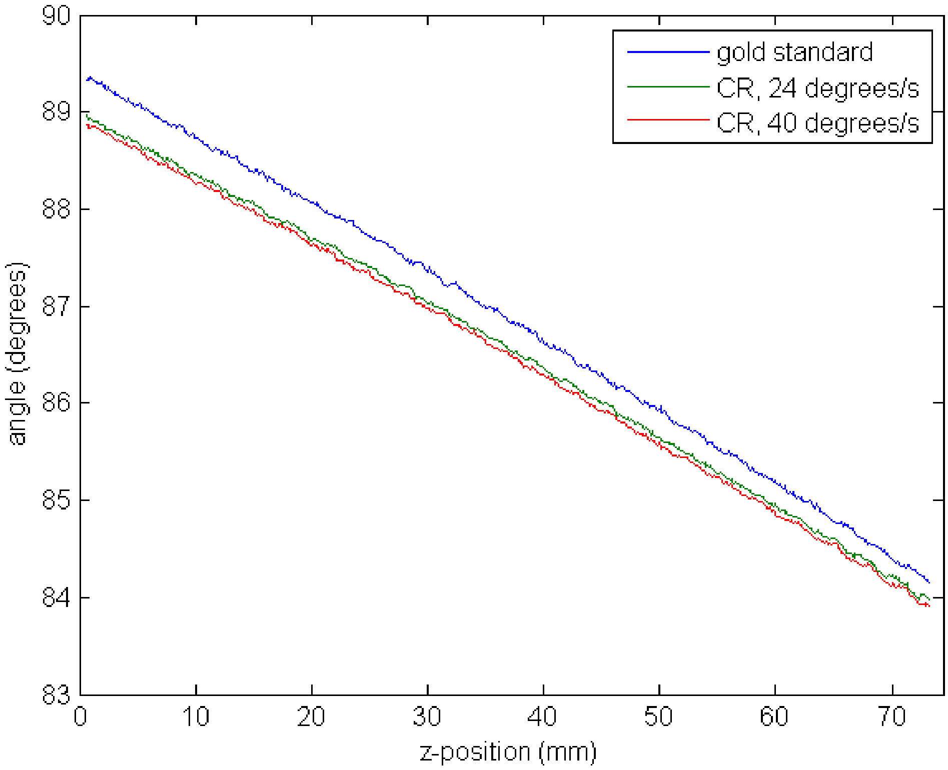

Figure 4.6: The angular positions of the pipe in the volumes reconstructed from the measurements given by Table 3.2. The angles are measured using the position of the center of mass of the pipe phantom compared to the center of rotation shown in Fig. 3.2.

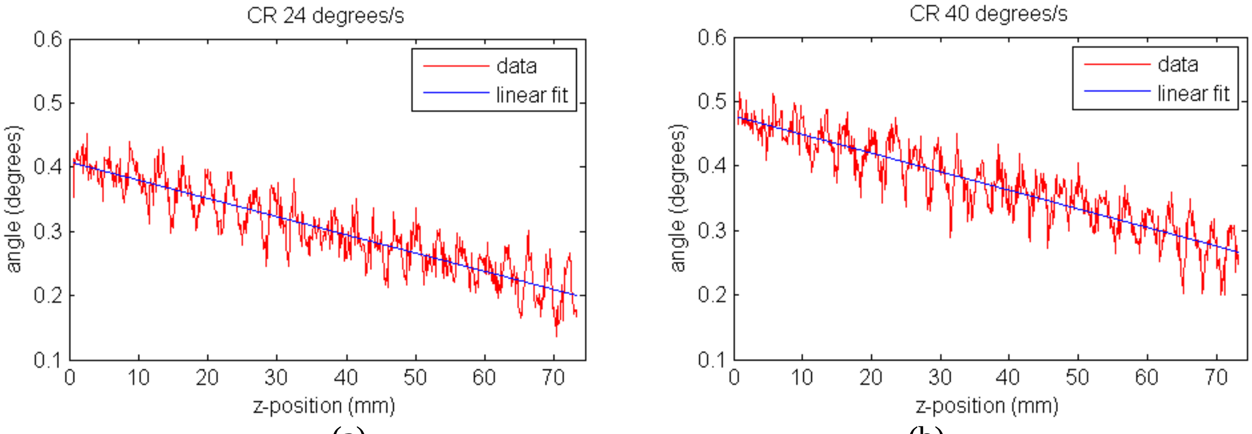

(a) (b)

Figure 4.7: The differences in angle between the Gold Standard and the measurement (a) #2, (b) #3 of Table 3.2. The blue line is a linear fit of the slope. The R^2 of the two fits are 0.82 and 0.81 respectively, this means the data fits linear regression model well.

Table 4.4: The ordinary least-squared estimates for the linear regression of the angle deformation as given in Eq. 4. The measurement column refers to the measurements given in Table 3.2.

Measurement	parameter	Mean	Standard Error	p-value	R^2
2	γ	-0.00284	5.51×10^{-5}	< .001	0.813
2	β	0.408	0.00239	< .001	
3	γ	-0.00288	5.62×10^{-5}	< .001	0.815
3	β	0.478	0.00239	< .001	

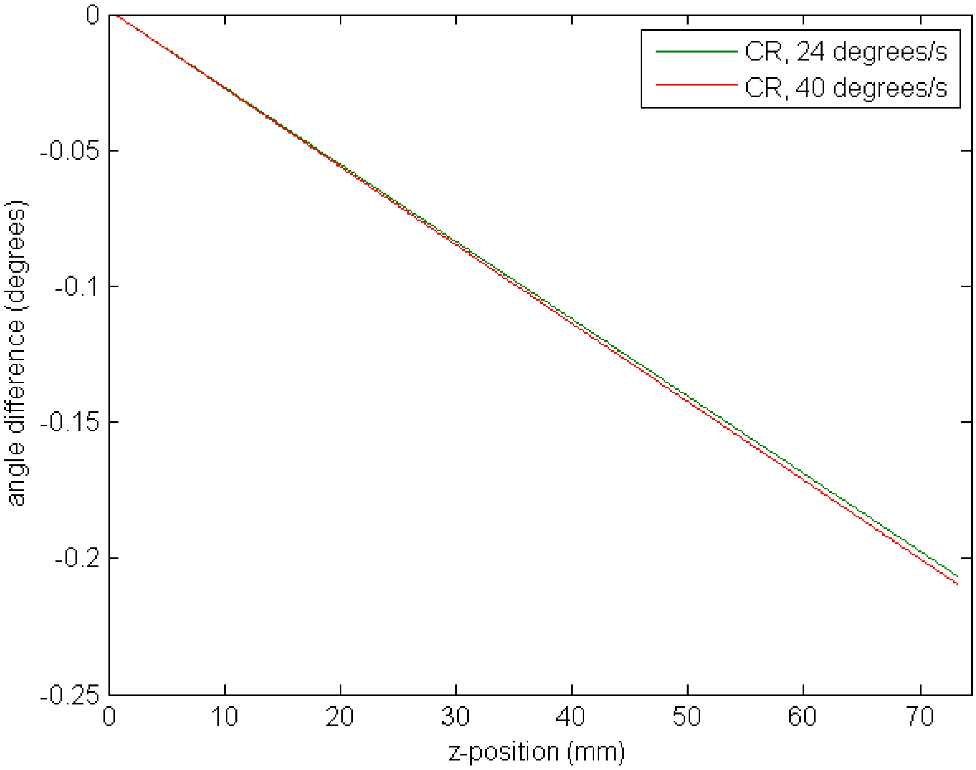

Figure 4.8: The twist of each volume as a function of the Z-position, the first slice is selected as the reference to which the angle difference is calculated.

5

Discussion

5.1. Acquisition Mode

Table 4.1 gives several direct differences between S&S and CR. First of all CR allows for the fastest total scan time; 15 seconds for a full rotation.

Measurements 6 and 9 can be used to determine the speed-up factor, as both are done using the same setting, the only difference is the rotation mode used. This resulted in a difference in scan time of a factor 4 (1 minute for S&S, while CR only took 15 s).

Image degradation was further investigated, by looking at the resulting images. The selected gold standard (Measurement 1) was compared to the quickest measurement (Measurement 8). Looking at Fig. 4.1, showing the results of the first projection of both measurements, there appears to be no visual differences between the measurements, although it must be noted that the gold standard has a 2x finer pixel grid thus possibly higher resolution. When looking Fig. 4.2 (transaxial slices of the reconstructed volumes of both measurements) real differences are visible: the transaxial slice of the gold standard is a clean, sharp image whereas the transaxial slice of measurement 8 is of lower quality. First of all, streak lines are visible which are resulting from the lower number of projections used, which leads to less angular data, which is needed for the best possible reconstruction. Furthermore, the details in the image are much less clear and the tissue-SNR is lower (7,9 dB instead of 10,8 dB); this is likely due to the lower resolution of the images and the lower number of projections used in reconstruction. To do faster CT a lower number of projections can be acquired and resolution is partly sacrificed. So when doing scans the trade-off between scan time (and thus radiation dose) and image quality needs to be taken into account. Very fast CT of up to 15 s for a complete scan is feasible but small anatomical details of the subject becomes more difficult to distinguish. This is very useful in tracking contrast agents through the subject, as the time in which a scan can be made determines the temporal resolution in tracking contrast agents. This time required for a full CT scan has decreased by a factor 27.7 (=6:55min/15s) between the gold standard and the quickest measurement.

5.2. Afterglow

The measured decay profile of the detector is given in Fig. 4.4. Note that as the X-ray source response is not instant, it could be that the X-ray source only started turning off somewhere after t=0. At the second measurement point (t=33 ms) the intensity has already dropped, so this means the X-ray source started turning off between t=0 and t=33 ms. Also note that the X-ray source does not turn off instantaneously so part of the decay profile measured might be actually due to the X-ray source turning off gradually.

For the gold standard of section 4.1 the time between each projection was 3.75 s, meaning that the afterglow will have no impact in measurements performed at these speeds. For the fastest scan done in section 4.1 the time between each projection is 0.104 s. According to Table 4.2 for this time interval, almost 7% of the original intensity is still present in the detector image. As the X-ray that is still not completely shut down also contributes to this value, the actual intensity resulting from the afterglow must be lower than this 7%. In the continuous rotation measurements done on both the mouse and the pipe phantom no influence of afterglow was observed. To gain more accurate afterglow results further measurements are needed using dedicated devices in which the impact of the X-ray source is reduced. A possible way to do this would be to include a very fast X-ray Shutter and use a lower power X-ray source.

5.3. The rolling shutter effect

Table 4.4 gives the angle difference, the maximum shift was 0.00288 degrees per mm. This shift corresponds to a volume twist of 0.232 degrees along 80 mm length in z-direction (field-of-view of the CT). For an mouse sized object (radius about 13 mm) scanned in this system, this will result in a maximal shift of about 0.053 mm. This shift is so small that it does not need correction. Furthermore, any form of correction will most likely lead to a higher image degradation due to errors introduced by interpolation. Table 4.4 shows that increasing the speed from 24 m/s to 40 m/s increases the angle difference by only $4x10^{-5}$ degree per mm. This is not the expected result, as the rotational speed is almost doubled, but the angle difference only increases by a very tiny amount. This could indicate that the angle difference of 0.00288 degrees is not solely caused by the rolling shutter effect but some other difference between the both continuous rotation measurements and the gold standard causes this angle difference. This difference could be due to a mechanical issue, such as a slight in-plane rotation of the detector caused by different tension in the gantry resulting from the different acquisition mode. However, even if the exact cause of the found angle difference is not known, the angle difference measured does not require a correction as the shift is too small to require a correction.

6

Conclusion

It was found that a reduction in scan time from 6:55 to 15 seconds was feasible using 2x2-binning continuous rotation instead of 1x1 binning continuous rotation, this did lead to a reduction in SNR from 10.8 dB to 7.9 dB. So the tradeoff between scan speed and image quality should be taking into account when performing a CT scan.

At the fastest image acquisitions speeds used in this report, afterglow might cause slight image degradation. After 103 ms, which is also the time intervals between acquiring projections during the 15 s scan (quickest scan done on the deceased mouse) 7% of the original intensity was measured in the detector. This could be partly caused by the shutdown behavior of the X-ray source, and no influence of afterglow was found in the other measurements. Hence, it is unlikely that afterglow causes serious image degradation at the speeds used in this report. However, further research should be done to better estimate the effect of Afterglow at these high acquisition speeds.

Volume twist due to the Rolling Shutter Effect does not require corrections at the speeds measured within this report, as the maximum volume twist was found to be 0.0029 degrees per mm, any correction will most likely lead to higher errors resulting from interpolation.

7

Acknowledgements

First of all, I would like to thank prof. Beekman for the opportunity to do this project. I owe a large debt of gratitude to Chao for the time and effort he put into this project, especially for providing an enormous amount of much needed feedback on this report. I would like to thank Janne for helping with the language and grammar in an early version of this report. N.B. any errors still present in the final version are solely of my own doing. I would also like to thank Jarno for helping me whenever I ran into difficulties while programming and the rest of RD&M for helping me with new ideas and making this project a more enjoyable experience.

References

[1] Brenner, D. J., and E. J. Hall. "Computed tomography—an increasing source of radiation exposure." *New England Journal of Medicine* 357.22 (2007): 2277-2284.

[2] Krauss B, Schmidt B, Flohr TG. Dual Source CT. In: Johnson TRC, Fink C, Schönberg SO, Reiser MF, eds. *Dual Energy CT in Clinical Practice*. Heidelberg: Springer, 2010:11-20.

[3] Lee, S. C., et al. "A flat-panel detector based micro-CT system: performance evaluation for small-animal imaging." *Physics in medicine and biology* 48.24 (2003): 4173.

[4] Paulus, M. J., et al. "High-resolution x-ray CT screening of mutant mouse models." *BiOS 2000 The International Symposium on Biomedical Optics*. International Society for Optics and Photonics, 2000.

[5] Paulus, M. J., et al. "High resolution X-ray computed tomography: an emerging tool for small animal cancer research." *Neoplasia* 2.1 (2000): 62-70.

[6] Goorden, M. C., et al. "VECTor: a preclinical imaging system for simultaneous submillimeter SPECT and PET." Journal of Nuclear Medicine 54.2 (2013): 306-312.

[7] Boone, J. M., O. Velazquez, and S. R. Cherry. "Small-animal X-ray dose from micro-CT." *Molecular imaging* 3.3 (2004): 149-158.

[8] Seeram, E. *Computed tomography: physical principles, clinical applications, and quality control*. Elsevier Health Sciences, 2013.

[9] Gupta, R, et al. "Flat-Panel Volume CT: Fundamental Principles, Technology, and Applications 1." *Radiographics* 28.7 (2008): 2009-2022.

[10] Konstantinidis, A. C., et al. "The Dexela 2923 CMOS X-ray detector: A flat panel detector based on CMOS active pixel sensors for medical imaging applications." *Nuclear Instruments and Methods in Physics Research Section A: Accelerators, Spectrometers, Detectors and Associated Equipment* 689 (2012): 12-21.

[11] Feldkamp, L. A., L. C. Davis, and J. W. Kress. "Practical cone-beam algorithm." *JOSA A* 1.6 (1984): 612-619.

[12] Schulze, R., et al. "Artefacts in CBCT: a review." *Dentomaxillofacial Radiology* (2014).

[13] Hsieh, J. "Computed tomography: principles, design, artifacts, and recent advances." Bellingham, WA: SPIE, 2009.

[14] Sharp, G. C., et al. "GPU-based streaming architectures for fast cone-beam CT image reconstruction and demons deformable registration." *Physics in medicine and biology* 52.19 (2007): 5771.

[15] Lavrent'ev, M. M., and M. M. Lavrentev, eds. *Computerized Tomography: Proceedings of the Fourth International Symposium, Novosibirsk, Russia*. VSP, 1995.

[16] Kerl, H. U., et al. "Evaluation of a continuous-rotation, high-speed scanning protocol for micro-computed tomography." *Journal of computer assisted tomography* 35.4 (2011): 517-523.

[17] "DEXELA 1207, 1512, 2307, 2315 and 2923 Flat Panel X-ray Detectors." Perkin Elmer. Web. 21 June 2015.

[18] Rit, S., et al. "The Reconstruction Toolkit (RTK), an open-source cone-beam CT reconstruction toolkit based on the Insight Toolkit (ITK)." *Journal of Physics: Conference Series*. Vol. 489. No. 1. IOP Publishing, 2014.

[19] Ibanez, L., et al. "The ITK software guide." (2003).

Appendix A: Correction methods

A.1. Afterglow Correction

Correcting for afterglow could be done by simply subtracting several of the previous images made from the last image acquired. To properly do this, a weight factor has to be applied to the previous images. This weighting factor is dependent on the amount of afterglow, or scintillator decay time and acquisition time. These weighting factors can be determined by simple measurements of the detector, exposing the scintillator to radiation for a short period of time, and then acquiring images with the X-ray source turned off. The decay profile can now be determined from the pixel intensity of the acquired images.

A.2. Rolling Shutter Effect Correction

At least two methods of correcting for the distortion caused by the rolling shutter effect are possible. The first is implementing a row by row reconstruction; the second is untwisting the reconstructed volume.

A.2.1. Row by row Reconstruction

This first method of correcting for the Rolling Shutter Effect is doing a row by row reconstruction. In normal reconstruction the volume is reconstructed by uploading an entire projection at the time and attributing a single angle to this projection. Because each row is read out in a consecutive order, each row in the projection corresponds to a slightly different angle with a constant angle increment between each row.

A method of correct volume reconstruction would be to upload only a single row at a time, attributing the correct angle for each row. This method of reconstruction limits the error due to the Rolling Shutter Effect to the uncertainty to which the angle increment between rows is known. Disadvantages of this correction method are the complexity of the implementation and the possible increase of the computational cost of doing the volume reconstruction.

A.2.2. Untwisting the Reconstructed Volume

Another possible method of correcting for the Rolling Shutter Effect is untwisting the reconstructed volume. As the Rolling Shutter Effect results in a twisted reconstructed volume, the reconstructed volume may be corrected by twisting the volume in the opposite direction of the original twist. As backprojection of the different rows does not result in a reconstructed volume where each slice only has a contribution from only one row (each slice has contributions from multiple rows), twisting the volume would only be an approximation. Also the uncertainty of the amount of twist in the reconstructed volume will lead to an error in this method. And the method of correction requires interpolation which will lead to blurring.